The EMBO Journal (2006) 25, 4728–4739 | © 2006 European Molecular Biology Organization | All Rights Reserved 0261-4189/06
www.embojournal.org

THE EMBO JOURNAL

In vivo phosphorylation of CFTR promotes formation of a nucleotide-binding domain heterodimer

Martin Mense[1], Paola Vergani[1,3], Dennis M White[1], Gal Altberg[1], Angus C Nairn[2] and David C Gadsby[1,*]

[1]Laboratory of Cardiac/Membrane Physiology, Rockefeller University, New York, NY, USA and [2]Department of Psychiatry, Yale University, New Haven, CT, USA

The human ATP-binding cassette (ABC) protein CFTR (cystic fibrosis transmembrane conductance regulator) is a chloride channel, whose dysfunction causes cystic fibrosis. To gain structural insight into the dynamic interaction between CFTR's nucleotide-binding domains (NBDs) proposed to underlie channel gating, we introduced target cysteines into the NBDs, expressed the channels in *Xenopus* oocytes, and used *in vivo* sulfhydryl-specific crosslinking to directly examine the cysteines' proximity. We tested five cysteine pairs, each comprising one introduced cysteine in the NH_2-terminal NBD1 and another in the COOH-terminal NBD2. Identification of crosslinked product was facilitated by co-expression of NH_2-terminal and COOH-terminal CFTR half channels each containing one NBD. The COOH-terminal half channel lacked all native cysteines. None of CFTR's 18 native cysteines was found essential for wild type-like, phosphorylation- and ATP-dependent, channel gating. The observed crosslinks demonstrate that NBD1 and NBD2 interact in a head-to-tail configuration analogous to that in homodimeric crystal structures of nucleotide-bound prokaryotic NBDs. CFTR phosphorylation by PKA strongly promoted both crosslinking and opening of the split channels, firmly linking head-to-tail NBD1–NBD2 association to channel opening.
The EMBO Journal (2006) **25,** 4728–4739. doi:10.1038/sj.emboj.7601373; Published online 12 October 2006
Subject Categories: membranes & transport; structural biology
Keywords: ABC transporter; bifunctional crosslinking; CFTR chloride channel; cysteine-free protein; NBD1–NBD2 complex

Introduction

The cystic fibrosis transmembrane conductance regulator (CFTR), encoded by the gene found mutated in cystic fibrosis patients (Riordan *et al*, 1989), is a member of the superfamily of ATP-binding cassette (ABC) transporter ATPases. Like most eukaryotic ABC proteins, CFTR comprises two transmembrane domains each linked to a cytoplasmic nucleotide-binding domain (NBD1, NBD2) (Figure 1). Unlike any other ABC protein, however, CFTR functions as a Cl^-- ion channel. Opening and closing of a CFTR channel, like the transport function of other ABC proteins, is regulated by ATP binding and hydrolysis at the NBDs. But, channel activity requires prior cAMP-dependent protein kinase (PKA)-mediated phosphorylation of the regulatory (R) domain that connects CFTR's two homologous halves (e.g., Gadsby and Nairn, 1999; Sheppard and Welsh, 1999).

Much is known about CFTR's role in epithelial function and about how CFTR channel activity is regulated (Kirk and Dawson, 2003), but little is known about CFTR structure. The sole exceptions are a low-resolution map from cryo-electron microscopy of 2D crystals of CFTR (Rosenberg *et al*, 2004), and high-resolution structures of NBD1 from mouse and human CFTR (Lewis *et al*, 2004, 2005; Thibodeau *et al*, 2005) that display the overall architecture, and arrangement of ATP-contacting 'Walker A and B' motifs and of the 'ABC signature' (LSGGQ) sequence, found in all other isolated NBD structures (e.g., Armstrong *et al*, 1998; Hung *et al*, 1998; Karpowich *et al*, 2001; Yuan *et al*, 2001).

Evidence from crystal structures of prokaryotic NBD homodimers (Hopfner *et al*, 2000; Smith *et al*, 2002; Chen *et al*, 2003; Zaitseva *et al*, 2005) and full transporters (Locher *et al*, 2002; Reyes and Chang, 2005), and from biochemical tests on intact prokaryotic (Fetsch and Davidson, 2002) or eukaryotic ABC transporters (Loo *et al*, 2002) suggests that NBD pairs may, at least transiently, form homodimeric complexes with two ATP binding sites within the dimer interface (for a review, see Higgins and Linton, 2004). In the homodimeric crystal structures, each ATP links the Walker motifs of one NBD to the signature sequence of the opposing NBD, in a rotationally symmetric head-to-tail dimer (Hopfner *et al*, 2000; Smith *et al*, 2002; Chen *et al*, 2003; Zaitseva *et al*, 2005). We have proposed that in CFTR a corresponding association between ATP-bound NBD1 and NBD2 accompanies opening of the ion channel (Vergani *et al*, 2003, 2005). We present here direct evidence, from sulfhydryl-specific crosslinking studies in living cells, that activation of human CFTR channels by phosphorylation promotes formation of a head-to-tail NBD1–NBD2 complex with an interface that mimics that found in homodimeric prokaryotic NBD crystals. Furthermore, by crosslinking during electrophysiological recordings, we demonstrate that the crosslinked NBD1–NBD2 complex characterizes an open-channel conformation of CFTR.

Results

Removal of native cysteines from CFTR

Before target cysteines for crosslinking could be introduced into CFTR, it was necessary to remove native cysteines to

*Corresponding author. Laboratory of Cardiac/Membrane Physiology, Rockefeller University, 1230 York Avenue, New York, NY 10021-6399, USA. Tel.: +1 212 327 8680; Fax: +1 212 327 7589;
E-mail: gadsby@rockefeller.edu
[3]Present address: Department of Pharmacology, University College London, London WC1E 6BT, UK

Received: 8 February 2006; accepted: 30 August 2006; published online: 12 October 2006

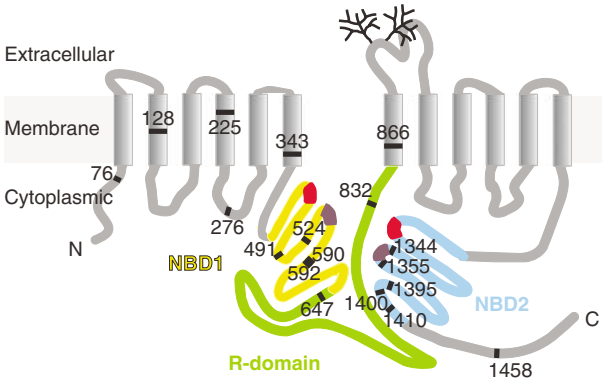

Figure 1 Native cysteines of human epithelial CFTR. Topological cartoon of CFTR showing the 18 cysteines indicated by their position numbers, the transmembrane domains (gray), the R domain (green), and the relative locations of Walker A (red) and ABC signature (purple) motifs in the nucleotide-binding domains, NBD1 (yellow) and NBD2 (cyan).

preclude their reaction with sulfhydryl reagents. We used PCR-based mutagenesis and/or gene synthesis techniques to replace all 18 native cysteines in human CFTR (Figure 1) with serines, one at a time or in groups. Functional expression of wild type (WT; Figure 2A, middle) and of mutant (e.g., Figure 2A, bottom) CFTR channels was assessed using two-microelectrode voltage-clamp recordings of forskolin-activated Cl^- currents in cRNA-injected *Xenopus* oocytes (e.g., Chan *et al*, 2000). Forskolin (the adenylyl cyclase agonist and hence stimulator of PKA activity) elicited robust responses in most mutant channels lacking one or more cysteines, including channels in which all of the cysteines except two (Cys 590 and 592 in NBD1) had been replaced by serines (16CS; Figure 2B and C). Functional expression was markedly diminished when C590 and C592 were both mutated to serine, regardless of whether the other 16 cysteines remained (data not shown) or had all been replaced by serines (Figure 2B, 16CS + C590S/C592S). Nor could C590 and C592 be replaced by alanine, threonine or phenylalanine (Figure 2B), but function was similar to that of the 16CS background when they were replaced by leucines (16CS + C590L/C592L; Figure 2A and B) or valines (16CS + C590V/C592V; Figure 2B). In excised patches, where [ATP] and PKA activity could be controlled

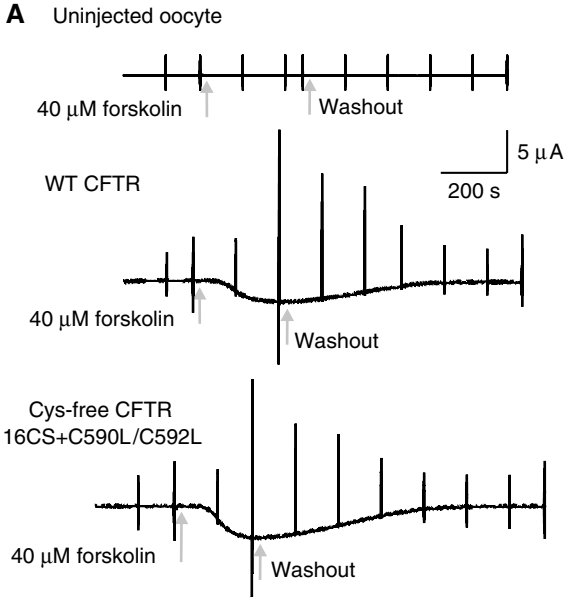

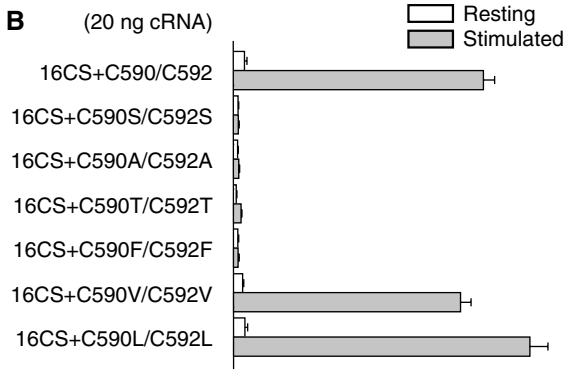

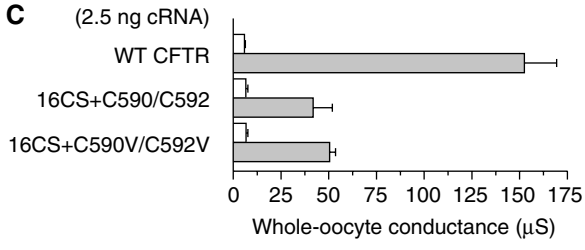

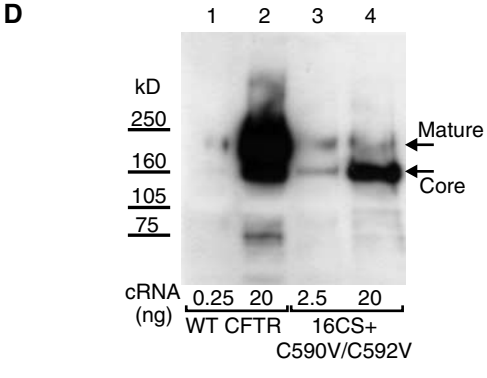

Figure 2 Expression and function of cysteine-deficient CFTR channels in *Xenopus* oocytes. (**A**) Two-microelectrode voltage-clamp current recordings from uninjected oocyte and oocytes expressing WT CFTR (2.5 ng cRNA) or HA-tagged Cys-free CFTR 16CS + C590L/C592L (20 ng cRNA); vertical current deflections monitor conductance, which was transiently increased by brief exposure to 40 μM forskolin (between arrows). (**B**) Summary of mean ± s.d. whole-oocyte conductances determined as in (A), before ('resting', white bars) and at maximal forskolin effect ('stimulated', gray bars), 3 days after injection of 20 ng cRNA encoding HA-tagged CFTR 16CS constructs containing native C590 and C592 or substitutions at those positions as indicated; forskolin elicited significant conductance only with C590 and C592 unchanged (131 ± 6 μS, $n = 3$), or replaced by valines (119 ± 6 μS, $n = 15$) or leucines (155 ± 9 μS, $n = 3$). (**C**) Conductances from oocytes injected with 2.5 ng cRNA, and measured 1 day later for WT (153 ± 17 μS, $n = 3$), or 3 days later for HA-tagged 16CS mutants with C590/C592 (42 ± 10 μS, $n = 6$) or C590V/C592 V (51 ± 3 μS, $n = 6$). This under-represents the functional difference between WT and mutants, as conductance is enhanced by injecting more cRNA or allowing more time for its expression. (**D**) WT CFTR and Cys-free CFTR (16CS + C590V/C592V) were immunoprecipitated from membranes of oocytes injected with cRNA amounts indicated, and subjected to SDS–PAGE and Western blot analysis; arrows mark core-glycosylated and mature fully glycosylated CFTR.

independently, Cys-free (16CS + C590V/C592V) CFTR channels, like WT, required phosphorylation by PKA before they could be opened by ATP, closed upon ATP removal, and were activated half-maximally by ~50 μM [ATP] (Supplementary Figure S1); their single-channel conductance was very slightly larger than that of WT CFTR channels.

Functional expression of CFTR correlates with the appearance of fully glycosylated CFTR protein (Gregory *et al*, 1991; Denning *et al*, 1992), and so we tested whether the smaller activated whole-oocyte conductance in intact oocytes expressing the mutants (Figure 2C) might reflect their impaired maturation. Western blotting of immunoprecipitated channels (Figure 2D) supported this interpretation. Oocytes injected with 20 ng WT CFTR cRNA yielded dense bands (Figure 2D, lane 2) of both core-glycosylated and fully glycosylated WT CFTR. But maturation of Cys-free CFTR was less efficient, and after injection of 20 ng Cys-free CFTR cRNA only a weak band corresponding to mature fully glycosylated CFTR could be detected (Figure 2D, lane 4) whereas a stronger signal reflected core-glycosylated protein (lower arrow).

Introduction of target cysteines for crosslinking studies

On the basis of crystal structures of nucleotide-bound prokaryotic NBD homodimers and of monomeric NBD1 F508A from human CFTR, we made a homology model of the anticipated CFTR NBD1–NBD2 complex (Figure 3; see Materials and methods). We then selected candidate pairs of positions for crosslinking across three different regions of the heterodimeric interface: the 'NBD2' composite catalytic site (comprising NBD2 Walker A and B motifs and NBD1 signature sequence), a central region, and the 'NBD1' composite site (including NBD1 Walker motifs and NBD2 signature sequence).

Introducing target cysteines into the NBDs of full-length Cys-free CFTR further impaired protein maturation (data not shown). We were nevertheless able to retain the benefit of a cysteine-free background by carrying out crosslinking experiments on split CFTR channels (Chan *et al*, 2000; Csanády *et al*, 2000), comprising a native NH_2-terminal half (amino acids 1–633, including all nine native cysteines) and a Cys-free COOH-terminal half (amino acids 634–1480, with nine Cys-to-Ser mutations), both of which expressed well and were readily detected in Westen blots (see below). After introduction of a target cysteine in each half, the COOH-terminal half channel contained only a single cysteine. Any observed sulfhydryl-specific crosslinking of NH_2- and COOH-terminal half channels could therefore be unequivocally ascribed to linkage via that target cysteine. In addition, the use of split channels enhanced the relative mobility shift upon crosslinking, thereby rendering the identification of crosslinked product unambiguous.

Target cysteines were introduced one at a time into the half channels in place of the following residues: S1248 in the NBD2 Walker A sequence and S549 in the NBD1 LSGGQ signature sequence; S605 in NBD1 and A1374 in NBD2, both in central positions of the putative dimer interface; A462 in the NBD1 Walker A and S1347 in LSHGH of NBD2. Comparatively inefficient crosslinking across the latter NBD1 composite site in early tests prompted introduction of additional cysteine pairs in that region, replacing S459 in NBD1 Walker A and V1379 in NBD2, and S434 in NBD1 and D1336 in NBD2.

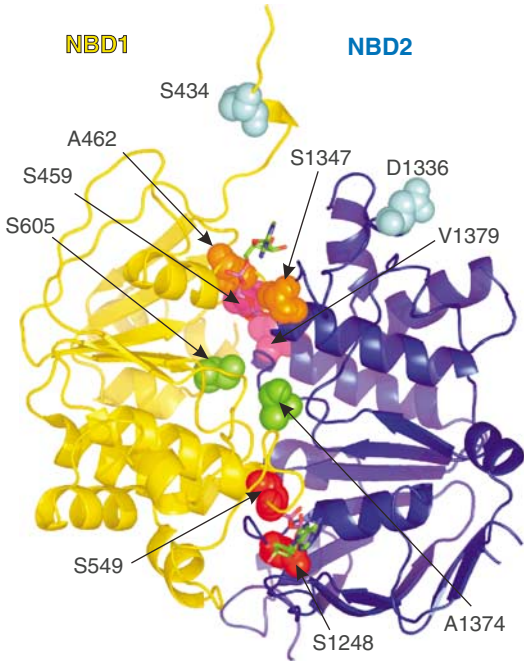

Figure 3 Homology model of a head-to-tail CFTR NBD1–NBD2 heterodimer, based on crystal structures of human CFTR NBD1 F508A and of ATP- or AMPPNP-bound NBDs of other ABC proteins (Materials and methods). Two ATP molecules (CPK-colored stick structures) are sandwiched between the Walker A and ABC signature sequences of opposing NBDs, NBD1 (yellow) and NBD2 (blue). To test this model by sulfhydryl-specific crosslinking, the residues in spacefill were mutated to cysteines in pairs, chosen so that an interfacial crosslink would span the 'NBD1' composite site (cyan, orange, and purple residue pairs), or a central region (green residues), or the 'NBD2' composite site (red residues). Due to sequence and structural differences between CFTR's NBD1 and other NBDs, the position of S434 is uncertain.

We confirmed that after introduction of each individual target cysteine, into either NH_2-terminal or Cys-free COOH-terminal half, co-expression in oocytes with the complementary half channel lacking introduced cysteines yielded mature fully glycosylated COOH-terminal CFTR halves in Western blots (broad band at ~130 kDa in Figure 4B, arrow; Figure 5, top row); some core-glycosylated COOH-terminal half-channel protein is also evident (sharp bands near 85 kDa in Figure 4B). The full glycosylation implies that the protein was correctly folded and trafficked to the surface membrane (Gregory *et al*, 1991; Denning *et al*, 1992; Chan *et al*, 2000). Accordingly, application of forskolin to raise PKA activity in oocytes expressing these split CFTR channels containing either one, or both, introduced target cysteines elicited robust increases in conductance (see Figures 4A and C); CFTR channels show low basal activity in resting oocytes, reflecting basally active PKA, but channel activity is enhanced several-fold upon stimulation of PKA by forskolin (Chan *et al*, 2000; Csanády *et al*, 2005). Similar split CFTR channels, though incorporating all native cysteines, were previously found to display basal and stimulated activity essentially like WT CFTR (Chan *et al*, 2000; Csanády *et al*, 2000). Comparable levels of expression (Figures 6–9 and Supplementary Figure S2) and function (e.g., Figure 4A and C) were obtained when both co-expressed half channels contained a target cysteine.

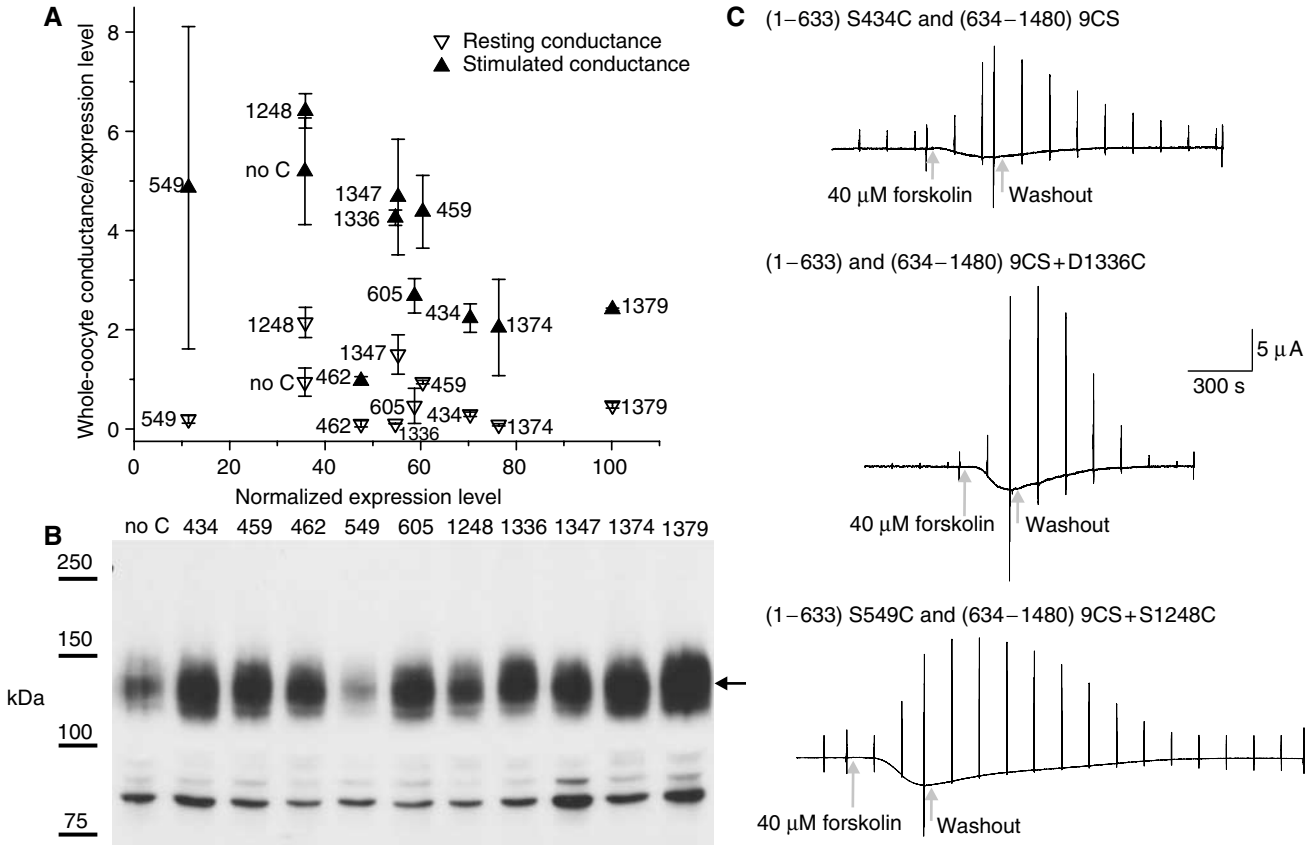

Figure 4 Expression (A, B) and function (A, C) of split CFTR channels containing introduced cysteines. Oocytes were injected with 5 + 5 ng cRNA encoding NH_2-terminal (1–633), and COOH-terminal (634–1480) 9CS (Ser replacing Cys at positions 647, 832, 866, 1344, 1355, 1395, 1400, 1410 and 1458), half channels containing either no introduced cysteine in NBD1 or NBD2 ('no C' label in A, B), or a single introduced cysteine at the residue position indicated beside each point in (A), above each lane in (B), and above each recording in (C). (**A**) Summary of resting and stimulated whole-oocyte conductances (μS) normalized to relative expression level, plotted against levels of expression (normalized to the highest measured value). (**B**) Expression levels were measured from a Western blot (anti-R-domain antibody) of ~25 μg of membrane proteins from 30 to 32 resting oocytes as gray level intensities of the broad bands of fully glycosylated COOH-terminal half channels (arrow); the lower sharp bands near 85 kDa are core-glycosylated COOH-terminal half channels. (**C**) Three examples of conductance measurements, at rest and after stimulation with 40 μM forskolin, in oocytes containing an introduced cysteine in NBD1 (top), or in NBD2 (middle), or in both NBDs (bottom).

Crosslinking tests

We assessed crosslinking of target cysteines by exposing intact oocytes, both at rest and after PKA stimulation by forskolin plus IBMX, to a membrane-permeant bismaleimide-based crosslinking reagent, bismaleimidoethane (BMOE) or bismaleimidohexane (BMH), and then analyzing membrane proteins by SDS–PAGE.

In control tests, oocytes expressing split CFTR channels containing only a single target cysteine were exposed to BMOE or BMH under optimal conditions (see below). Western blots with an anti-R-domain antibody identified both core-glycosylated (~85 kDa, poorly phosphorylated; ~90 kDa after strong phosphorylation by PKA) and fully glycosylated (~130 kDa) COOH-terminal half channels (Figure 5, top row), and blots of the same membranes with anti-NH_2-terminal antibody showed the NH_2-terminal half channels (~55 kDa; Figure 5, bottom row). However, the blots show no BMOE- or BMH-induced bands that are detected with both antibodies and so provide no evidence for crosslinking between any introduced cysteine in NBD2 and a native cysteine in the NH_2-terminal half channel. The lack of strong bands of higher molecular mass in either blot indicates that there was no efficient crosslinking of introduced target cysteines to each other, offering no convincing evidence for the presence of homodimeric half-channel complexes. Nonetheless, occasional faint BMOE- and/or BMH-induced bands are discernible in Figure 5 (and to varying extents also in Figures 6–9), usually confined to the blots with the anti-NH_2-terminal antibody. These largely indistinct unidentified bands (arrows in Figure 5) likely reflect crosslinking of the more reactive NH_2-terminal half channels (due to its nine native cysteines) to other proteins, possibly in oligomeric complexes.

'NBD2' composite site, with S549C and S1248C

In contrast to these results with single introduced cysteines, BMOE (flexible spacer, reactive groups ⩽8 Å apart) or BMH (flexible spacer length, 16 Å) application to oocytes co-expressing CFTR half channels (1–633) S549C and (634–1480) 9CS + S1248C, with both target cysteines in the NBD2 composite catalytic site (Figure 3), yielded a clear crosslinked product (Figure 6, arrows labeled X-link) not seen without crosslinking reagent (lanes 1 and 9). The product band detected with antibody against the NH_2-terminal half channel was of identical molecular mass to that identified with antibody against the COOH-terminal half channel, strongly sug-

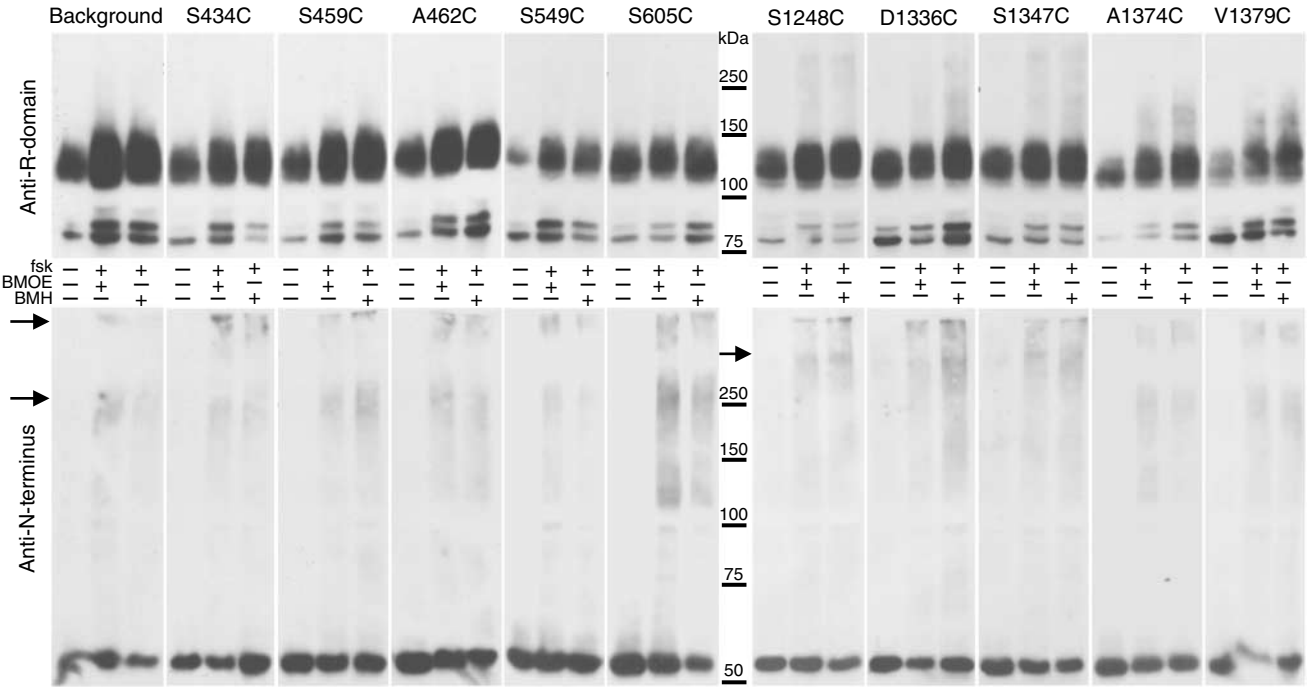

Figure 5 The absence of efficient crosslinking when no, or only one, engineered cysteine is present. Oocytes injected with 5 + 5 ng cRNA encoding NH_2-terminal (1–633), and COOH-terminal (634–1480) 9CS, half channels containing no (background), or just one, introduced cysteine in either NBD1 or NBD2, at the position indicated above each panel. Oocytes were untreated, or pretreated with 40 μM forskolin plus 1 mM IBMX and then incubated with 300 μM BMOE or 600 μM BMH at room temperature, as indicated. Membrane proteins were analyzed by SDS–PAGE and blotted with antibody against the R domain (COOH-terminal half-channel, upper blots) or antibody against the NH_2-terminus (lower blots). Note that upon forskolin treatment, phosphorylation of the R domain slows mobility of the COOH-terminal half channel (Csanády *et al*, 2005) resulting in the appearance of a sharp band (at ~90 kDa) just above the ~85 kDa core-glycosylated band. No strong high-molecular-mass band, reflecting crosslinked product, is evident in any lane, but arrows mark weak, dispersed, unidentified BMOE- and/or BMH-induced bands discernible in some blots with antibody against the NH_2-terminus.

gesting that the two half channels were crosslinked. The crosslinked product migrated with an apparent molecular mass (~250 kDa) slightly higher than that of linear, full-length, mature CFTR protein (~200 kDa; Figure 2D). We estimated crosslink yield as the fractional intensity of crosslinked product signal relative to the sum of signal intensities of crosslinked product plus fully glycosylated, but non-crosslinked, monomer; strengthening of the crosslinked product signal was generally associated with a corresponding loss of signal in the fully glycosylated monomer band (Figures 6–9). The efficiency of crosslinking appeared similar for BMOE and BMH, and was somewhat higher when carried out at 23°C (lanes 2–5, 10–14) than on ice (lanes 6, 7, 14 and 15).

Importantly, although crosslinking was observed in resting oocytes (lanes 2, 4, 10 and 12), after stimulation of PKA activity by preincubation of oocytes with 40 μM forskolin plus 1 mM IBMX (phosphodiesterase inhibitor, to sustain elevated [cAMP]), the yield of crosslinked product was increased several-fold (e.g., compare lane 10 with 11, 12 with 13). Preincubation of oocytes with forskolin and IBMX alone (without crosslinking reagent) yielded no crosslinked product bands (Supplementary Figure S3).

Central region, with S605C and A1374C

Similar results were obtained with the pair of cysteines introduced at positions 605 and 1374, predicted to lie near the center of the proposed NBD1–NBD2 interface. A crosslinked product with apparent molecular mass of ~220 kDa was evident (Figure 7, arrows labeled X-link) in lanes from oocytes incubated with BMOE or BMH at room temperature or on ice (lanes 2–7 and 9–14), but not from untreated oocytes (lanes 1 and 8). The same molecular mass product band was detected with antibodies against epitopes in the NH_2-terminal or the COOH-terminal half channel. PKA stimulation again resulted in a strong, several-fold, increase in crosslinking yield (compare lane 2 with 3, 4 with 5, 9 with 10, and 11 with 12).

'NBD1' composite site, with A462C and S1347C, S459C and V1379C, and S434C and D1336C

At the NBD1 composite site, we first examined crosslinking between positions homologous to those tested successfully at the NBD2 composite site. However, crosslinking between position 462 in NBD1 Walker A and position 1347 in NBD2 LSHGH sequence was weak, although still apparently enhanced upon PKA stimulation (Figure 8A; compare lane 10 with 11, 12 with 13). Concerned that this weak crosslink signal might reflect steric hindrance by the ATP believed to remain bound at the NBD1 composite site for prolonged periods (Basso *et al*, 2003), we introduced two additional pairs of target cysteines near this site. One pair, at positions 459 in NBD1 and 1379 in NBD2, showed robust crosslinking with either BMOE or BMH (Figure 8B) and, once again, crosslinking yield was increased several-fold after stimulation of PKA with forskolin and IBMX (e.g., compare lane 2 with 3, or 9 with 10). Crosslinking was weaker, but still evident,

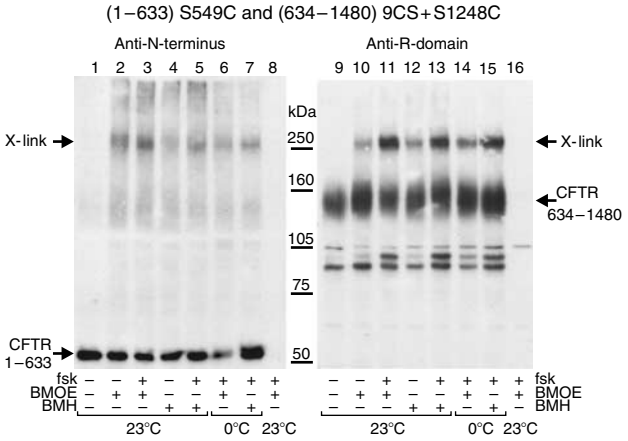

Figure 6 Crosslinking across the 'NBD2' composite catalytic site, between position 1248 in NBD2 Walker A and position 549 in NBD1 LSGGQ. Western blots identify the NH_2-terminal half channel (1–633), S549C (left panel; lower arrow), the COOH-terminal half channel (634–1480) 9CS + S1248C (right panel; core-glycosylated, ~85–90-kDa, bands; fully glycosylated, lower arrow), and crosslinked product (both panels; arrows labeled X-link). Incubation temperature, presence or absence of 300 μM BMOE or 600 μM BMH, and/or treatment with 40 μM forskolin plus 1 mM IBMX ('fsk') are indicated below each lane. Forskolin increased the yield of crosslinked product four-fold for BMOE and two-fold for BMH. Samples in lanes 8 and 16 are from uninjected control oocytes.

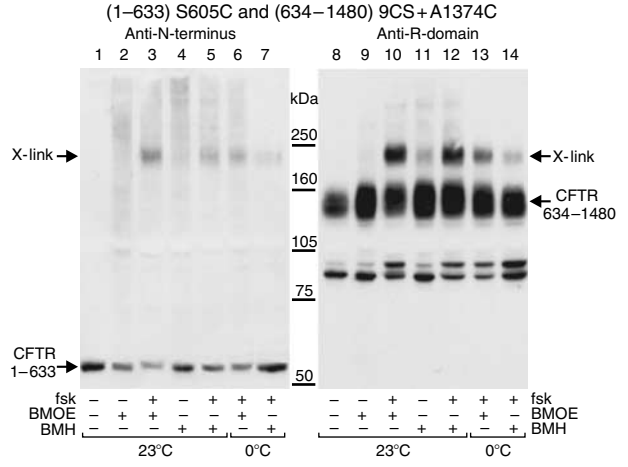

Figure 7 Crosslinking between central region residues, 605 of NBD1 and 1374 of NBD2. Western blots show CFTR half channels (1–633) S605C (left panel; lower arrow), (634–1480) 9CS + A1374C (right panel; core-glycosylated, ~85–90 kDa, bands; fully glycosylated, lower arrow), and crosslinked product (both panels; arrows labeled X-link). Incubation temperature, presence or absence of 300 μM BMOE or 600 μM BMH, and/or treatment with 40 μM forskolin plus 1 mM IBMX ('fsk') are indicated below each lane. Forskolin increased the yield of crosslink product 870-fold for BMOE and four-fold for BMH.

when carried out on ice (lanes 6, 7, 13 and 14). The other cysteine pair, at positions 434 in NBD1 and 1336 in NBD2, yielded crosslinked product only with the longer crosslinker BMH (Figure 8C, lanes 5, 7, 12 and 14) but not with BMOE (lanes 3, 6, 10 and 13), in contrast to all other pairs described so far. That crosslink was obtained both at room temperature and on ice and, like other crosslinks, was enhanced upon stimulation of PKA activity.

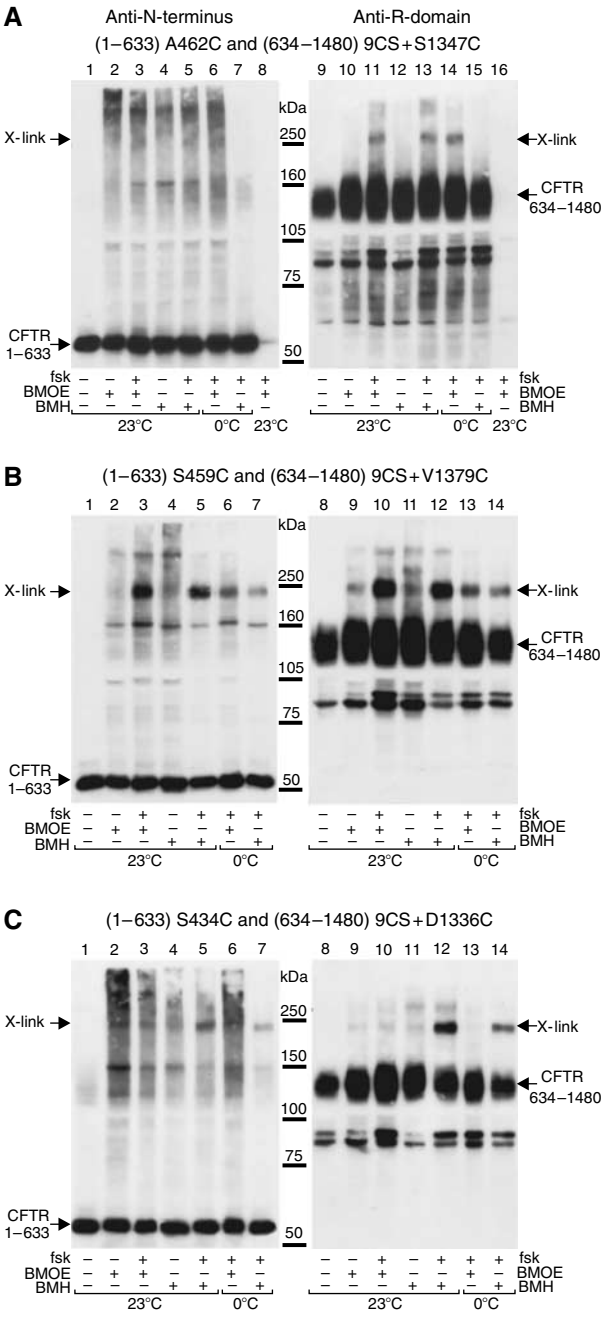

Figure 8 Crosslinking across the 'NBD1' composite site. Incubation temperature, presence or absence of 300 μM BMOE or 600 μM BMH, and/or treatment with 40 μM forskolin plus 1 mM IBMX ('fsk') are indicated below each lane in all panels. Left panels show NH_2-terminal half channels (lower arrows), right panels show COOH-terminal half channels (core-glycosylated, ~85–90-kDa bands; fully glycosylated, lower arrows), and all panels show crosslinked product (upper arrows labeled X-link); some other BMOE- and/or BMH-induced bands, mostly in the blots with anti-NH_2-terminal antibody, likely reflect crosslinking of NH_2-terminal half channels (with nine native Cys) to unknown proteins. (**A**) CFTR half channels (1–633) A462C (left panel) and (634–1480) 9CS + S1347C (right panel). Forskolin increased the yield of crosslinked product >1000-fold for both BMOE and BMH; lanes 8 and 16 are samples from uninjected oocytes. (**B**) CFTR half channels (1–633) S459C (left panel) and (634–1480) 9CS + V1379C (right panel). Forskolin increased crosslink product yield nine-fold for BMOE and 5-fold for BMH. (**C**) CFTR half channels (1–633) S434C (left panel) and (634–1480) 9CS + D1336C (right panel), as well as crosslinked product (arrow labeled X-link, both panels). Forskolin increased crosslink product yield 9-fold for BMH. Crosslink yield for BMOE was negligibly small.

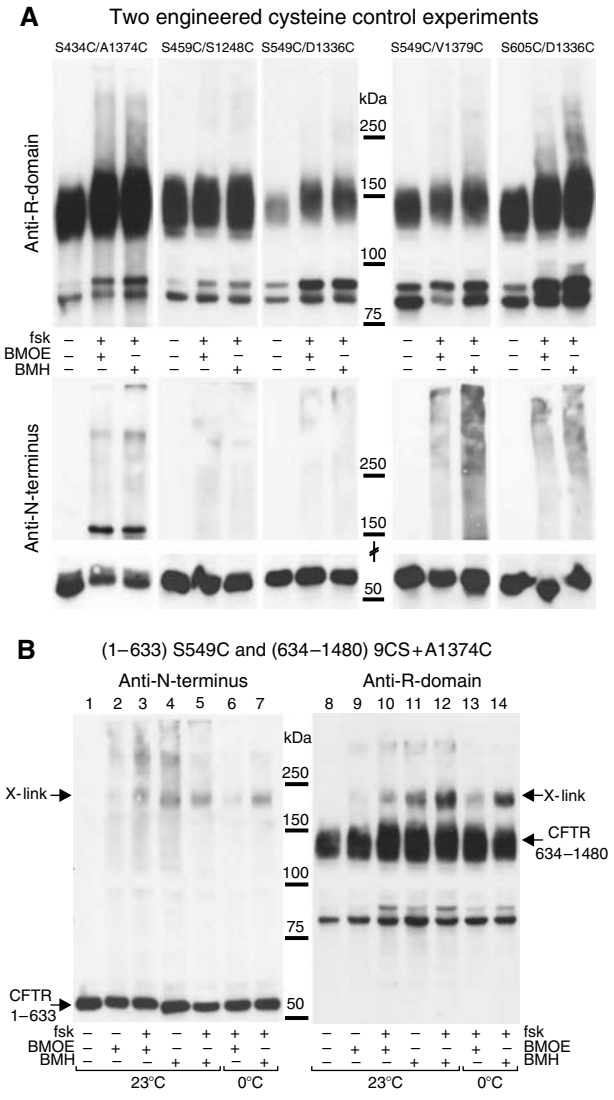

Figure 9 Tests of crosslinking between NBD1 and NBD2 using other combinations of the target cysteines. The presence or absence of 300 μM BMOE or 600 μM BMH and/or treatment with 40 μM forskolin plus 1 mM IBMX ('fsk') are indicated for each lane in all panels. (**A**) Oocytes were injected with cRNAs encoding NH_2-terminal (1–633) and COOH-terminal (634–1480) 9CS half channels, each containing one introduced cysteine, in the combinations indicated above each panel. Incubations were at room temperature. Western blots identify NH_2-terminal half channels (lower rows) and core- and fully glycosylated COOH-terminal half channels (upper row). (**B**) Western blots show CFTR half channels (1–633) S549C (left panel, lower arrow) and (634–1480) 9CS + A1374C (right panel, core-glycosylated, ~85–90-kDa bands; fully glycosylated, lower arrow), as well as crosslinked product (both panels, arrows labeled X-link). Incubation temperature is indicated below each lane. Forskolin increased the yield of crosslink product eight-fold for BMOE and two-fold for BMH.

In addition to these specific crosslink products recognized by antibodies to both half channels, Figure 8 shows other BMOE- and/or BMH-induced bands, predominantly in the blots with anti-NH_2-terminal antibody. Because some migrate at a molecular mass overlapping that of fully glycosylated COOH-terminal half channels, we cannot discern whether these reflect crosslinked complexes of NH_2-terminal half channels with COOH-terminal halves (complexes somehow truncated, or core-glycosylated) or with unidentified proteins.

Tests with other combinations of NBD1 and NBD2 introduced cysteines

To test the specificity of the interfacial crosslinks established in Figures 6–8, we co-expressed six different pairs of the same target cysteines, again one in NBD1 and one in NBD2 in split CFTR channels, but now in new combinations. For five of these new pairs, C434 with C1374, C459 with C1248, C605 with C1336, C549 with C1336, and C549 with C1379, no crosslinked product was obtained with either BMOE or BMH (Figure 9A) after prior stimulation of the oocytes by forskolin and IBMX. The predicted distances (from Figure 3) between these target cysteine pairs range from 28 Å for the C605/C1336 pair to 39 Å for the pair C549/C1336. In contrast, the sixth pair, C549 (in NBD1 LSGGQ) with C1374 (in NBD2 center), predicted to lie 13 Å apart, could be crosslinked by the 16 Å-spanning BMH, but were relatively resistant to the shorter (8 Å) reagent BMOE (Figure 9B).

Functional consequences of crosslinking across the 'NBD2' composite site

To determine the functional consequence of crosslinking across the NBD1–NBD2 interface, as described above, we recorded macroscopic currents in inside-out patches excised from *Xenopus* oocytes expressing split CFTR channels while applying crosslinking reagents. Unfortunately, BMOE and BMH both diminished currents in control split channels, comprising (1–633) and (634–1480) 9CS, that lacked target cysteines, presumably by reacting with native cysteines in the NH_2-terminal halves. We therefore turned to oxidative crosslinking with Cu(II)(*o*-phenanthroline)$_2$, which in the presence of molecular oxygen can catalyze disulfide bond formation between the sulfur atoms of two sufficiently close thiols (Kobashi, 1968). Although no residual current was seen when 200 μM Cu(II)(*o*-phenanthroline)$_2$ was added during withdrawal of ATP from split CFTR channels containing only one target cysteine, either S549C (Figure 10A and D) or S1248C (Figure 10B and D), in patches containing both half channels (1–633) S549C and (634–1480) 9CS + S1248C, a substantial persistent current was observed (Figure 10C and D). That residual current was nucleotide-independent, but was abolished by 15 mM DTT (Figure 10C), which is expected to reduce disulfide bonds, and had an average amplitude about 20% of the maximal current activated by 5 mM ATP plus 300 nM PKA catalytic subunit (Figure 10D).

Discussion

Crosslinking results and models of NBD interaction

The positions of the six distinct crosslinks between target cysteines in NBD1 and NBD2 demonstrated here (summarized in Figure 11) provide concrete evidence that, in fully functional CFTR (Figure 4; compare with Figure 2 and Supplementary Figure S1), NBD1 and NBD2 form a head-to-tail 'heterodimeric' complex, analogous to prokaryotic NBD homodimers found in crystal structures (Hopfner *et al*, 2000; Smith *et al*, 2002; Chen *et al*, 2003; Zaitseva *et al*, 2005). The six include three crosslinks across the NBD1 composite site (between the NBD1 head, containing the Walker motifs, and the NBD2 tail, containing the ABC signature sequence: C462–C1347, C459–C1379, and C434–C1336), one crosslink between central regions of NBD1 and NBD2 (C605–C1374), one crosslink between the NBD1-tail

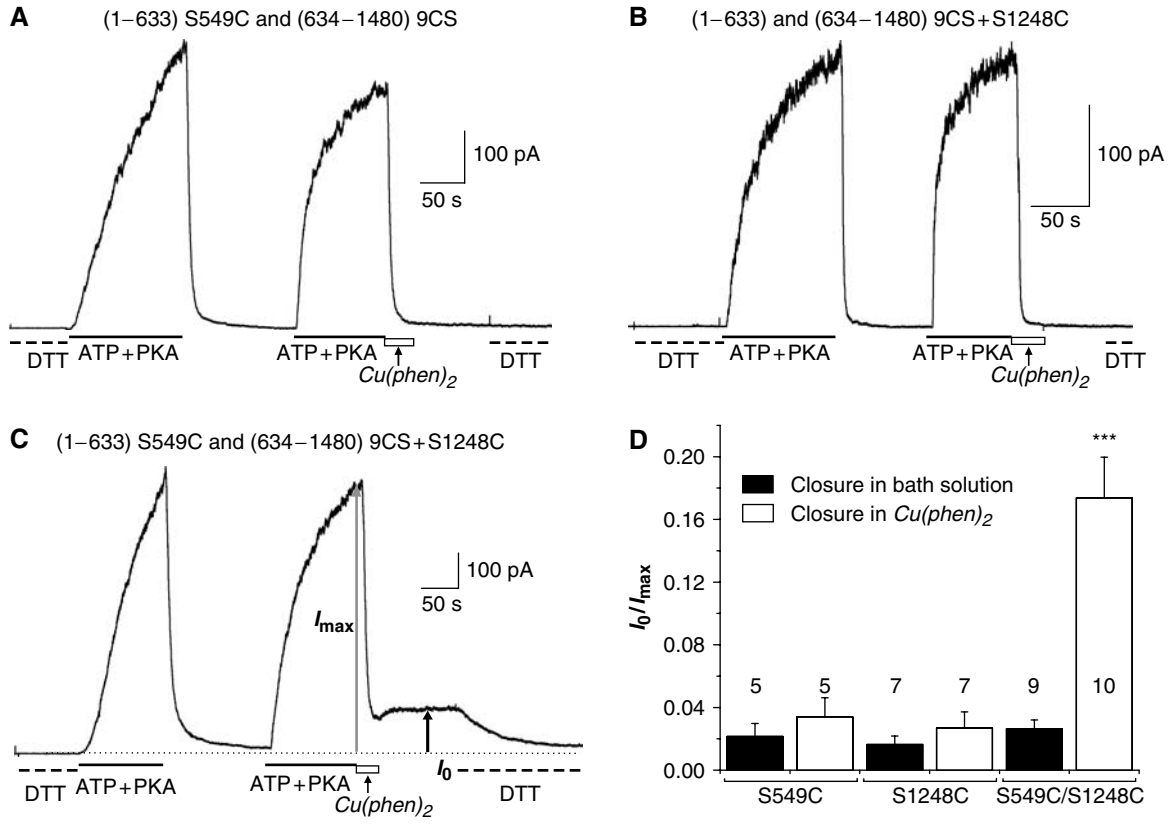

Figure 10 Functional consequence of crosslinking S549C to S1248C. (**A–C**) Currents activated by 5 mM ATP and 300 nM PKA catalytic subunit in thousands of split CFTR channels in inside-out patches excised from oocytes expressing NH_2-terminal (1–633), and COOH-terminal (634–1480) 9CS, half channels containing only one target cysteine, S549C (A) or S1248C (B), or both S549C and S1248C (C). Current decay due to channel closure on washout of ATP and PKA was unaltered by Cu(II)(*o*-phenanthroline)$_2$ when channels contained only one target cysteine (A, B), but resulted in a stable nucleotide-independent, but DTT-sensitive, residual current I_0 (C, black arrow). (**D**) Average (±s.e.m.) amplitude of I_0 normalized to the maximal (ATP-plus PKA-activated) current, I_{max}, for split channels as in (A–C); number of measurements is indicated for each column. For S549C/S1248C channels I_0/I_{max} is significantly different (***$P \leqslant 0.0005$, Student's *t*-test) after closure in the presence of Cu(II)(*o*-phenanthroline)$_2$ compared to its absence (bath solution).

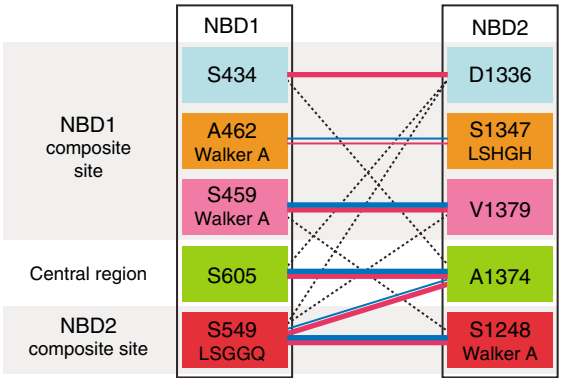

Figure 11 Summary of crosslinking results. Residues replaced by target cysteines in NBD1 (left column) are paired with those in NBD2 (right column) such that horizontal connections between boxes of identical color represent the crosslinks formed between the original five target pairs. Red connecting lines join positions crosslinked with BMH, and blue lines represent crosslinks with the shorter BMOE. Thinner lines, for example, between A462 and S1347, indicate weaker crosslink signals. Black dashed lines connect pairs of positions that could not be crosslinked with either BMOE or BMH.

signature sequence and the NBD2 center (C549–C1374), and a final crosslink across the NBD2 composite site, between the signature sequence in the NBD1 tail and the Walker A sequence in the NBD2 head (C549–C1248). Except for the C434/C1336 pair, for which structural disparity between CFTR's NBD1 (Lewis *et al*, 2004) and other NBDs precludes specification of the position of S434 and hence meaningful distance determination, the homology model in Figure 3 suggests sulfur-to-sulfur distances of 13 Å for C549/C1374 and 7.5–9.5 Å for the other cysteine pairs, in accord with our observation of crosslinking with 8 Å- (BMOE) and/or 16-Å-spanning (BMH) bifunctional sulfhydryl-specific reagents. In all cases, the crosslinked product was identified both with an antibody to the NBD1-containing half channel and with an antibody to the NBD2-containing half. Relatively low efficiency of the crosslink across the NBD1 composite site, from position 462 in the NBD1 Walker A motif to position 1347 in the NBD2 LSHGH signature sequence might be attributable to protracted occupancy of that site by tightly bound ATP (cf Szabo *et al*, 1999; Aleksandrov *et al*, 2002; Basso *et al*, 2003), which would be expected to interfere with access of the crosslinking reagents to the target cysteines.

Notably, we found no crosslinking (Figures 9A and 11) between NBD1 head and NBD2 head (or NBD2 center), nor between NBD2 tail and NBD1 tail (or NBD1 center). Nor did we find convincing evidence for 'homodimeric' interactions of NBD1 or of NBD2 (Figures 5–9): for example, we saw no efficient crosslinking between two NH_2-terminal half chan-

nels containing C605 (Figure 5, 7 and 9A), or two COOH-terminal half channels containing C1374 (Figure 5, 7, 9A and B), the two central positions tested. Moreover, we established that the presence or absence of crosslinked product was not correlated with expression levels of the half channels (Supplementary Figure S2), confirming the specificity of the observed crosslinks.

Head-to-tail dimeric NBD interactions in other ABC proteins are similarly supported by biochemical data. Thus, UV-dependent vanadate-mediated photocleavage of MalK domains in intact vanadate-arrested maltose transporters occurred selectively within signature sequences and Walker A sequences (Fetsch and Davidson, 2002), demonstrating that catalytic sites include both motifs, in accord with structures of ATP-bound NBD homodimers (e.g., Hopfner *et al*, 2000; Smith *et al*, 2002; Chen *et al*, 2003; Zaitseva *et al*, 2005). In addition, cysteine pairs introduced into the human multidrug transporter P-glycoprotein at sites equivalent to positions 549 and 1248 of CFTR's NBD2 composite catalytic site, and 462 and 1346 of CFTR's NBD1 site, could be oxidatively crosslinked, forming a disulfide bond (Cα separation of 5–8 Å), in the presence of copper phenanthroline (Loo *et al*, 2002). Both disulfide links could form after prolonged exposures to copper phenanthroline in the absence of ATP and at 4°C (Loo *et al*, 2002). Although this is somewhat surprising, given that equivalent residues are 15–20 Å apart in nucleotide-free structures of MalK NBDs (Chen *et al*, 2003) or intact BtuCD (prokaryotic vitamin B_{12} transporter; Locher *et al*, 2002), we also observed some crosslinking during 30-min incubations with bifunctional reagents on ice (Figures 6–9). Presumably, even at low temperature and/or without nucleotide the NBDs visit, if infrequently, conformations that permit crosslinking.

State dependence of crosslinking

A common feature of the crosslinks demonstrated here (Figures 6–9) is that, when oocytes were stimulated with 40 μm forskolin and 1 mM IBMX before exposure to the crosslinking reagents, the yield of crosslinked product increased ~5-fold on average (ignoring apparently infinite ratios due to weak resting signals). The fold increase in crosslink yield paralleled the forskolin/IBMX-induced increase in the phosphorylated fraction of the COOH-terminal half-channel (containing the R domain), indicated by the increased relative intensity of the upper versus lower band in the ~85–90-kDa doublet seen in Western blots with anti-R-domain antibody (Figures 5–9). These bands correspond to poorly phosphorylated (lower) and strongly phosphorylated (upper; e.g., Csanády *et al*, 2005) forms of the core-glycosylated half-channel. Comparable fractional increases in phosphorylation status may be expected for the fully glycosylated forms, although their greatly broadened bands tend to obscure the accompanying mobility shifts. As the same forskolin/IBMX treatment also results in a several-fold enhancement of CFTR conductance in oocytes expressing split CFTR channels harboring the various target cysteines (Figure 4A and C), we can conclude that crosslinking efficiency correlates not only with phosphorylation of CFTR but also with channel activity, that is, with open probability (e.g., Chang *et al*, 1993; Csanády *et al*, 2005). We then further conclude that the probability of CFTR assuming a conformation comprising a heterodimeric NBD1–NBD2 complex, along the lines modeled in Figure 3, is higher while the channel is open than when it is closed, as proposed (Vergani *et al*, 2003, 2005).

Functional consequences of crosslinking

The nucleotide-independent residual current induced by Cu(II)(*o*-phenanthroline)$_2$ in the split channels comprising (1–633) S549C and (634–1480) 9CS + S1248C (Figure 10C) provides direct evidence that artificial stabilization of the NBD1–NBD2 heterodimer tends to keep the affected channels open. Detailed characterization of that stabilized open state must await further analysis, but preliminary recordings from patches containing few Cu(II)(*o*-phenanthroline)$_2$-modified channels show that the disulfide bond between S549C and S1248C results in a high channel open probability in the absence of ATP, with a persistent open state repeatedly interrupted by temporary closures. The relatively small amplitude of the residual current (~20% of the maximal PKA-plus ATP-activated current; Figure 10C and D), therefore, presumably reflects the even smaller fraction of thiols that yield disulfide bonds (Careaga and Falke, 1992) in open channels during exposure to Cu(II)(*o*-phenanthroline)$_2$ while the channels are closing after ATP withdrawal. These results more directly demonstrate that the NBD1–NBD2 heterodimer configuration of CFTR is associated with the open channel state (Vergani *et al*, 2003, 2005).

Crosslinking data and NBD1 crystal structures

The recent structures of NBD1 monomers from mouse and human CFTR (Lewis *et al*, 2004, 2005; Thibodeau *et al*, 2005) could not entirely be incorporated into an NBD1–NBD2 heterodimer model (e.g., Figure 3) as they contain structural elements, absent from NBDs of other ABC proteins, that preclude close approach of NBD2 (Lewis *et al*, 2004). Because those elements include PKA consensus sequences they were called 'regulatory insertion' and 'regulatory extension', and it was suggested that their movement upon phosphorylation might permit NBD1–NBD2 interaction and hence explain activation of CFTR channel gating. In both mouse and human NBD1 crystals, the regulatory extension obscures position 605 (Lewis *et al*, 2004, 2005), and so would be expected to prevent crosslinking of a cysteine at that position to any residue in NBD2, in contrast to our demonstration of crosslinking between cysteines in positions 605 in NBD1 and 1374 in NBD2 (Figure 7). We therefore conclude that, in functioning CFTR channels, the regulatory extension must at least some of the time adopt a position distinct from those found so far in NBD1 crystals.

Expression of cysteine-free CFTR

Because we could replace any of CFTR's 18 native cysteines (individually or in groups) without preventing forskolin activation of robust Cl^- currents in oocytes expressing the resulting full-length mutant CFTR channels, we can conclude that no single cysteine is essential for CFTR channel trafficking or function. Even CFTR channels lacking all 18 cysteines showed, like WT CFTR, ATP-dependent gating that required prior phosphorylation by PKA (Figure 2; Supplementary Figure S1). Nevertheless, maturation of cysteine-free CFTR was substantially impaired (Figure 2D). This need not be surprising since cysteines equivalent to WT CFTR's C524, C590, C1355 and C1395 are well conserved in ABC-C subfamily homologs (closely related to CFTR; e.g., Dassa and

Bouige, 2001; Dean *et al* 2001) from yeast to mammals, and hence likely contribute importantly to native protein structure. Some impairment of processing has also been reported for cysteine-free mutants of more distantly related ABC proteins like P-glycoprotein (Loo and Clarke, 1995) and the *Escherichia coli* maltose transporter (Samanta *et al*, 2003).

Although substitution by similarly sized serine was well tolerated for 16 of CFTR's 18 cysteines, simultaneous replacement of both C590 and C592 by serines, threonines or alanines precluded functional expression. Surprisingly, introduction of larger but less polar side chains, for example, valine (residue volume, 105 $Å^3$; Creighton, 1992) or leucine (124 $Å^3$), at positions 590 and 592 improved CFTR maturation and function, whereas the even larger phenylalanine side chains (135 $Å^3$) were not tolerated. This pattern would be understandable if C590 and C592 were buried among hydrophobic residues, but that suggestion is not supported by the CFTR NBD1 structures (Lewis *et al*, 2004, 2005; Thibodeau *et al*, 2005) in which C592, at least, was found exposed on the domain surface. In addition, in the structures of the full transporters BtuCD (Locher *et al*, 2002) and MsbA (Reyes and Chang, 2005) residues homologous to C590 and C592 do not appear to directly contact the transmembrane domain in a manner that might bury their side chains. These cysteines could be needed for interactions along maturation or trafficking pathways, but a reasonable speculation is that Cys 592, found in all CFTR NBD1 sequences but in almost no other ABC-C-family sequence, might interact with the R domain, found only in CFTR.

Our demonstration here, that CFTR Cl^- channels devoid of all 18 native cysteines nevertheless retain many functional characteristics of WT, establishes cysteine-free CFTR as a useful tool for further work on CFTR structure and mechanism (e.g., Wang *et al*, 2005; Liu *et al*, 2006).

Materials and methods

Molecular biology

De novo PCR gene synthesis (Stemmer *et al*, 1995) and site-directed mutagenesis (QuikChange, Stratagene, La Jolla, CA, USA) were combined to generate cysteine-free, 18CS, CFTR. All cDNAs were cloned into the pGEMHE plasmid as described (Chan *et al*, 2000). CFTR with substitutions C128S, C225S, C343S and C866S was provided by Dr DC Dawson (OHSU, Portland, OR, USA). Primers for the mutations C76S, C276S and C832S are listed in Table I. We replaced 11 cysteines in two segments of CFTR by synthesizing cDNAs using Pfu turbo DNA polymerase (Stratagene, La Jolla, CA, USA): CFTR bases 1445–2007 (NBD1syn), encoding residues 482–669 (replacing 5 cysteines), and bases 3991–4443 (NBD2syn), encoding residues 1331-stop codon (replacing 6 cysteines). An *Eag*I site introduced at CFTR bases 1455–1460 (primer in Table I) was used with the native *Bsg*I site (bases 1961–1966) to subclone fragment NBD1syn into the full-length gene. NBD2syn was subcloned between the native *Tth111*I site (bases 4006–4014) and a *Bst*EII site following the stop codon. Substitutions at C590 and C592 were made by site-directed mutagenesis (primers in Table I). The entire sequence of full-length cysteine-free CFTR (16CS + C590/592L) is available from Genbank (#AY608405).

Primers for cysteine insertions S434C, S459C, A462C, S549C, S605C, S1248C, D1336C, S1347C, A1374C and V1379C are given in Table I. The CFTR half channels (1–633) and cysteine-free (634–1480) 9CS were generated essentially as described (Chan *et al*, 2000). Half channels with engineered cysteines were obtained either by site-directed mutagenesis or by subcloning appropriate cDNA fragments from full-length CFTR mutants. NH_2-terminal HA epitope tags were introduced into cysteine-mutant CFTR constructs by site-directed mutagenesis (primer in Table I).

Point mutations and PCR-synthesized cDNA fragments were confirmed by automated sequencing. cDNA constructs were linearized using the *Nhe*I site in the pGEMHE plasmid and transcribed with the T7 mMessage mMachine RNA kit (Ambion, Austin, TX, USA).

Whole-oocyte and excised-patch current recording

Xenopus laevis oocytes isolated as described (Chan *et al*, 2000) were injected one day later with cRNAs in 50 nl volumes. For whole-oocyte current recording, oocytes in a flow chamber were superfused with oocyte Ringer solution (82.5 mM NaCl, 2 mM KCl, 1 mM $MgCl_2$, 5 mM HEPES, pH 7.5), impaled with two 3-M KCl-filled microelectrodes, and held at −50 mV. One hundred ms steps to voltages from −80 to + 100 mV, in 20 mV increments, were applied before, during and after exposure to 40 μM forskolin to activate CFTR Cl^- channels. Linear regression fits to plots of steady currents against step voltage gave whole-oocyte conductances, reported as mean ± s.d. of $\geqslant 3$ measurements (except $n = 2$ in Figure 4A). Unitary CFTR channel currents were recorded in inside-out excised patches exposed to MgATP, after channel activation by catalytic subunit of PKA, and channel gating kinetics were analyzed as described (Vergani *et al*, 2003). For recording macroscopic currents of split CFTR channels in excised patches (Figure 10), oocytes were

Table I Forward primers for site-directed mutagenesis PCR

C76S	5′-GCCCTTCGGCGATcgTTTTTCTGGAG-3′
C276S	5′-CTGTTAAGGCCTACTcCTGGGAAGAAGC-3′
C832S	5′-CGAAGAAGACCTTAAGGAGTcCTTTTTTGATGATATGGAGAGC-3′
EagI site	5′-GGTAAAATTAAGCACAGcGGccGAATTTCATTCTGTTCTC-3′
HA epitope	5′-CGGGCCGCCATGtAcccatAcGACGttccgGAttAcgcaAGGTCGCCTCTGG-3′
CFTR 16CS C590A/C592A	5′-GGAGATCTTCGAGAGCgCTGTCgCTAAACTGATGGC-3′
CFTR 16CS C590F/C592F	5′-GGAGATCTTCGAGAGCTtTGTCTtTAAACTGATGGC-3′
CFTR 16CS C590L/C592L	5′-GGAGATCTTCGAGAGCctTGTCctTAAACTGATGGC-3′
CFTR 16CS C590T/C592T	5′-GGAGATCTTCGAGAGCaCTGTCaCTAAACTGATGGC-3′
CFTR 16CS C590V/C592V	5′-GGAGATCTTCGAGAGCgtcGTCgtTAAACTGATGGC-3′
S434C	5′-CCTCTTCTTCAGTAATTCTgtCTaCTTGGTACTCCTGTC-3′
S459C	5′-GTTGGCGGTTGCTGGATgCACTGGAGCAGGCAAG-3
A462C	5′-GCTGGATCCACTGGGtgcGGCAAGACTTCACTTC-3′
L549C	5′-GGTGGAATCACACtatGcGGAGGTCAACGAGCACG-3′
S605C	5′-GGATTTTGGTCACaTgTAAAATGGAAC-3′
S1248C	5′-CCTCTTGGGAAGAACCGGtTgtGGGAAGAGTAC-3′
D1336C	5′-GTTTCCTGGGAAGCTTtgCTTTGTCCTTGTGG-3′
L1346C	5′-GGATGGGGGCTCTGTCTgtAGTCATGGCCACAAGC-3′
A1374C	5′-GATGAACCAAGCtgTCATTTAGATCC-3′
V1379C	5′-GCTCATTTAGATCCgtgcACATACCAAATAATTCG-3′

The underlined bases are the codons for the introduced serines, cysteines or other residues; lowercase letters mark base changes from the original sequence, including those for introducing diagnostic restriction endonuclease sites. For all PCR reactions the reverse primers were exact complements of these forward primers.

injected with cRNA encoding NH_2- and COOH-terminal half-channels (20 ng each) and recordings were made 5–6 days later under the conditions used for unitary channel current measurements.

Immunoprecipitation of CFTR

Four days after injection with 0.25–20 ng cRNA (Figure 2), 20 oocytes for each condition were homogenized by sonication in 500 μl modified RIPA buffer (0.5% Triton X-100, 0.5% NP-40, 0.5% Na-deoxycholate, 0.2% SDS, 150 mM NaCl, 50 mM Tris–HCl pH 7.2, 1 mM PMSF, protease inhibitor cocktail), the cell homogenate solubilized for 30 min at 4°C, and the insoluble fraction pelleted at 18 000 *g* for 30 min and discarded. The supernatant was incubated overnight at 4°C with mouse monoclonal anti-CFTR antibody MM13-4 (Upstate Biotechnologies, Lake Placid, NY, USA) at 1:100 dilution. Antibody–protein complexes were collected with protein A/G beads (Santa Cruz Biotechnologies, Santa Cruz, CA, USA), washed three times with RIPA buffer and, just before SDS–PAGE, CFTR was eluted during a 20-min incubation at 37°C in Laemmli buffer containing 200 mM DTT.

Crosslinking of CFTR half channels

Oocytes were injected with, typically, 5 ng cRNA each of NH_2-terminal (1–633) and cysteine-free COOH-terminal (634–1480) CFTR half channels, containing engineered cysteines as specified. Two or three days later, 25–35 intact oocytes equilibrated in 4 ml Ringer plus 1.8 mM Ca^{2+} in a 35-mm Petri dish, on ice or at room temperature (~23°C), were exposed to membrane-permeant crosslinkers, bismaleimidoethane (BMOE, 300 μM) or bismaleimidohexane (BMH, 600 μM) (Pierce Biotechnology, Rockford, IL, USA). After 12 min incubation at 23°C, or 30 min on ice, oocytes were transferred to 500 μl ice-cold quenching solution (400 mM KCl, 5 mM HEPES, 25 mM L-cysteine, 300 mM sucrose, protease inhibitors, pH 7.0) and immediately homogenized by sonication (Branson Digital Sonifier 450, Branson, Danbury, CT, USA). When indicated, 40 μM forskolin plus 1 mM IBMX were added to activate CFTR 8 min before oocytes were exposed to crosslinkers.

Under conditions optimized for specific crosslinking, the yield of crosslinked product, migrating near the mass of full-length CFTR, was typically in the range of 20% (crosslinked product signal intensity as percent of the sum of signal intensities of crosslinked product plus fully glycosylated, non-crosslinked, monomer). Several mechanisms likely conspired to limit that yield: (i) crosslink yields for bifunctional reagents are limited by competing, unproductive reaction of the two target cysteines with two different bifunctional reagent molecules (Wu and Kaback, 1997; van Montfort *et al*, 2002); (ii) BMH and BMOE (both lipophilic) were applied to intact oocytes and had to pass through the membrane to reach their cytoplasmic targets, where their concentration could not be controlled; (iii) hydrolysis of maleimide groups in solution may render some bifunctional reagent molecules ineffective as crosslinkers; (iv) native cysteines in NH_2-terminal half channels might have permitted their crosslinking to unknown proteins, other than COOH-terminal half channels, and accumulation in massive complexes.

Oocyte plasma membrane preparation

Oocyte plasma membranes were prepared as described (Perez *et al*, 1994). The 20:50% interface of the sucrose gradient was collected, diluted 1:2 in phosphate-buffered saline (PBS) and membranes were pelleted by centrifugation at 50 000 *g* for 45 min, resuspended in PBS (5 μl/oocyte) with protease inhibitors, and analyzed by SDS–PAGE either immediately or after storage at −80°C. Contribution of intracellular membranes to this preparation is not excluded.

Western blot analysis and quantification

Total membrane protein concentrations (typically ~2 μg/μl; range 1.6–2.4 μg/μl) were determined with bicinchonic acid (Pierce Biotechnology, Rockford, IL, USA), and ~25 μg protein per lane (unless otherwise specified) were separated by SDS–PAGE on 6.5% gels, and transferred to Biorad PVDF membranes by semidry blot. Full-length CFTR and COOH-terminal half channels (634–1480) were detected with a rabbit polyclonal anti-R-domain antibody, G449, at 1:1000 dilution from stock (Picciotto *et al*, 1992); NH_2-terminal half channels (1–633) were detected with MM13-4 antibody (1:1000 dilution from stock, see above). HRP-conjugated secondary antibodies were goat anti-rabbit IgG (1:40 000; #A-0545, Sigma, St Louis, MO, USA) or goat anti-mouse IgG (1:20 000; #715-035-150, Jackson ImmunoResearch Laboratories, West Grove, PA, USA); immunoreactive bands were visualized with ECL Plus (Amersham, Piscataway, NJ, USA) and Kodak BioMax MR films (Kodak, Rochester, NY, USA). For quantification by densitometry (e.g., Figure 4A), since the linear range of ECL signal density is <10-fold, we exposed chemiluminescent membranes to film for varying times to ensure that signals stayed within the linear range. The resulting Western blot films were scanned at 16-bit grayscale resolution on a flatbed-scanner (Epson Perfection 3200 Photo, Epson, Long Beach, CA, USA) and gray level intensities measured with MetaMorph software (Molecular Devices, Sunnyvale, CA, USA).

Generation of homology model

The model of Figure 3 was built with Modeller (Sali and Blundell, 1993), which calculates homology models by satisfying structural restraints. Structural alignments were created including only ATP- (or AMPPNP-) bound NBD structures (HisP, PDB ID 1B0U (Hung *et al*, 1998); MJ0796, 1L2T (Smith *et al*, 2002); MalK, 1Q12 (Chen *et al*, 2003); GlcV, 1OXV (Verdon *et al*, 2003) and HlyB, 1XEF (Zaitseva *et al*, 2005), as well as human CFTR NBD1 F508A, 1XMI (Lewis *et al*, 2005). CFTR's NBD1 and NBD2 sequences were aligned to these structures, and the resulting alignments were manually adjusted, according to Pfam alignments of NBDs (http://www.sanger.ac.uk/cgi-bin/Pfam), and used to build a homology model of a CFTR NBD1–NBD2 heterodimer. The final image was rendered with PyMol (DeLano Scientific, http://www.pymol.org).

Supplementary data

Supplementary data are available at *The EMBO Journal* Online (http://www.embojournal.org).

Acknowledgements

We thank Nazim Fataliev for technical support. The work was supported by NIH Grant DK-51767 (to DCG). M Mense was partly supported by a fellowship from the Revson/Winston Foundation.

References

Aleksandrov L, Aleksandrov AA, Chang XB, Riordan JR (2002) The first nucleotide binding domain of cystic fibrosis transmembrane conductance regulator is a site of stable nucleotide interaction, whereas the second is a site of rapid turnover. *J Biol Chem* **277:** 15419–15425

Armstrong S, Tabernero L, Zhang H, Hermodson M, Stauffacher C (1998) Powering the ABC transporters: the 2.5 Å crystal structure of the ABC domain of RBSA. *Pediatr Pulm* **17:** 91–92

Basso C, Vergani P, Nairn AC, Gadsby DC (2003) Prolonged nonhydrolytic interaction of nucleotide with CFTR's NH_2-terminal nucleotide binding domain and its role in channel gating. *J Gen Physiol* **122:** 333–348

Careaga CL, Falke JJ (1992) Thermal motions of surface a-helices in the D-galactose chemosensory receptor. *J Mol Biol* **226:** 1219–1235

Chan KW, Csanády L, Seto-Young D, Nairn AC, Gadsby DC (2000) Severed molecules functionally define the boundaries of the cystic fibrosis transmembrane conductance regulator's NH(2)-terminal nucleotide binding domain. *J Gen Physiol* **116:** 163–180

Chang XB, Tabcharani JA, Hou YX, Jensen TJ, Kartner N, Alon N, Hanrahan JW, Riordan JR (1993) Protein kinase A (PKA) still activates CFTR chloride channel after mutagenesis of all 10 PKA consensus phosphorylation sites. *J Biol Chem* **268:** 11304–11311

Chen J, Lu G, Lin J, Davidson AL, Quiocho FA (2003) A tweezers-like motion of the ATP-binding cassette dimer in an ABC transport cycle. *Mol Cell* **12:** 651–661

Creighton TC (1992) *Proteins: Structures and Molecular Properties*. New York: WH Freeman

Csanády L, Chan KW, Seto-Young D, Kopsco DC, Nairn AC, Gadsby DC (2000) Severed channels probe regulation of gating of cystic fibrosis transmembrane conductance regulator by its cytoplasmic domains. *J Gen Physiol* **116:** 477–500

Csanády L, Seto-Young D, Chan KW, Cenciarelli C, Angel BB, Qin J, McLachlin DT, Krutchinsky AN, Chait BT, Nairn AC, Gadsby DC (2005) Preferential phosphorylation of R-domain serine 768 dampens activation of CFTR channels by PKA. *J Gen Physiol* **125:** 171–186

Dassa E, Bouige P (2001) The ABC of ABCS: a phylogenetic and functional classification of ABC systems in living organisms. *Res Microbiol* **152:** 211–229

Denning GM, Anderson MP, Amara JF, Marshall J, Smith AE, Welsh MJ (1992) Processing of mutant cystic fibrosis transmembrane conductance regulator is temperature-sensitive. *Nature* **358:** 761–764

Dean M, Rzhetsky A, Allikmets R (2001) The human ATP-binding cassette (ABC) transporter superfamily. *Genome Res* **11:** 1156–1166

Fetsch EE, Davidson AL (2002) Vanadate-catalyzed photocleavage of the signature motif of an ATP-binding cassette (ABC) transporter. *Proc Natl Acad Sci* **99:** 9685–9690

Gadsby DC, Nairn AC (1999) Control of CFTR channel gating by phosphorylation and nucleotide hydrolysis. *Physiol Rev* **79:** S77–S107

Gregory RJ, Rich DP, Cheng SH, Souza DW, Paul S, Manavalan P, Anderson MP, Welsh MJ, Smith AE (1991) Maturation and function of cystic fibrosis transmembrane conductance regulator variants bearing mutations in putative nucleotide-binding domains 1 and 2. *Mol Cell Biol* **11:** 3886–3893

Higgins CF, Linton KJ (2004) The ATP switch model for ABC transporters. *Nat Struct Mol Biol* **11:** 918–926

Hopfner KP, Karcher A, Shin DS, Craig L, Arthur LM, Carney JP, Tainer JA (2000) Structural biology of Rad50 ATPase: ATP-driven conformational control in DNA double-strand break repair and the ABC-ATPase superfamily. *Cell* **101:** 789–800

Hung LW, Wang IX, Nikaido K, Liu PQ, Ames GF, Kim SH (1998) Crystal structure of the ATP-binding subunit of an ABC transporter. *Nature* **396:** 703–707

Karpowich N, Martsinkevich O, Millen L, Yuan YR, Dai PL, MacVey K, Thomas PJ, Hunt JF (2001) Crystal structures of the MJ1267 ATP binding cassette reveal an induced-fit effect at the ATPase active site of an ABC transporter. *Structure* **9:** 571–586

Kirk KL, Dawson DC (eds) (2003) *The Cystic Fibrosis Transmembrane Conductance Regulator*. New York, NY, USA: Kluwer Academic/Plenum Publishers

Kobashi K (1968) Catalytic oxidation of sulfhydryl groups by *o*-phenanthroline copper complex. *Biochem Biophys Acta* **158:** 239–245

Lewis HA, Buchanan SG, Burley SK, Conners K, Dickey M, Dorwart M, Fowler R, Gao X, Guggino WB, Hendrickson WA, Hunt JF, Kearins MC, Lorimer D, Maloney PC, Post KW, Rajashankar KR, Rutter ME, Sauder JM, Shriver S, Thibodeau PH, Thomas PJ, Zhang M, Zhao X, Emtage S (2004) Structure of nucleotide-binding domain 1 of the cystic fibrosis transmembrane conductance regulator. *EMBO J* **23:** 282–293

Lewis HA, Zhao X, Wang C, Sauder JM, Rooney I, Noland BW, Lorimer D, Kearins MC, Conners K, Condon B, Maloney PC, Guggino WB, Hunt JF, Emtage S (2005) Impact of the {Delta}F508 mutation in first nucleotide-binding domain of human cystic fibrosis transmembrane conductance regulator on domain folding and structure. *J Biol Chem* **280:** 1346–1353

Liu X, Alexander C, Serrano J, Borg E, Dawson DC (2006) Variable reactivity of an engineered cysteine at position 338 in cystic fibrosis transmembrane conductance regulator reflects different chemical states of the thiol. *J Biol Chem* **281:** 8275–8285

Locher KP, Lee AT, Rees DC (2002) The *E. coli* BtuCD structure: a framework for ABC transporter architecture and mechanism. *Science* **296:** 1091–1098

Loo TW, Bartlett MC, Clarke DM (2002) The 'LSGGQ' motif in each nucleotide-binding domain of human P-glycoprotein is adjacent to the opposing Walker A sequence. *J Biol Chem* **277:** 41303–41306

Loo TW, Clarke DM (1995) Membrane topology of a cysteine-less mutant of human P-glycoprotein. *J Biol Chem* **270:** 843–848

Perez G, Lagrutta A, Adelman JP, Toro L (1994) Reconstitution of expressed KCa channels from *Xenopus* oocytes to lipid bilayers. *Biophys J* **66:** 1022–1027

Picciotto MR, Cohn JA, Bertuzzi G, Greengard P, Nairn AC (1992) Phosphorylation of the cystic fibrosis transmembrane conductance regulator. *J Biol Chem* **267:** 12742–12752

Reyes CL, Chang G (2005) Structure of the ABC transporter MsbA in complex with ADP.vanadate and lipopolysaccharide. *Science* **308:** 1028–1031

Riordan JR, Rommens JM, Kerem B, Alon N, Rozmahel R, Grzelczak Z, Zielenski J, Lok S, Plavsic N, Chou JL (1989) Identification of the cystic fibrosis gene: cloning and characterization of complementary DNA. *Science* **245:** 1066–1073

Rosenberg MF, Kamis AB, Aleksandrov LA, Ford RC, Riordan JR (2004) Purification and crystallization of the cystic fibrosis transmembrane conductance regulator (CFTR). *J Biol Chem* **279:** 39051–39057

Sali A, Blundell TL (1993) Comparative protein modelling by satisfaction of spatial restraints. *J Mol Biol* **234:** 779–815

Samanta S, Ayvaz T, Reyes M, Shuman HA, Chen J, Davidson AL (2003) Disulfide cross-linking reveals a site of stable interaction between C-terminal regulatory domains of the two MalK subunits in the maltose transport complex. *J Biol Chem* **278:** 35265–35271

Sheppard DN, Welsh MJ (1999) Structure and function of the CFTR chloride channel. *Physiol Rev* **79:** S23–S45

Smith PC, Karpowich N, Millen L, Moody JE, Rosen J, Thomas PJ, Hunt JF (2002) ATP binding to the motor domain from an ABC transporter drives formation of a nucleotide sandwich dimer. *Mol Cell* **10:** 139–149

Stemmer WP, Crameri A, Ha KD, Brennan TM, Heyneker HL (1995) Single-step assembly of a gene and entire plasmid from large numbers of oligodeoxyribonucleotides. *Gene* **164:** 49–53

Szabo K, Szakacs G, Hegeds T, Sarkadi B (1999) Nucleotide occlusion in the human cystic fibrosis transmembrane conductance regulator. Different patterns in the two nucleotide binding domains. *J Biol Chem* **274:** 12209–12212

Thibodeau PH, Brautigam CA, Machius M, Thomas PJ (2005) Side chain and backbone contributions of Phe508 to CFTR folding. *Nat Struct Mol Biol* **12:** 10–16

van Montfort BA, Schuurman-Wolters GK, Wind J, Broos J, Robillard GT, Poolman B (2002) Mapping of the dimer interface of the *Escherichia coli* mannitol permease by cysteine cross-linking. *J Biol Chem* **277:** 14717–14723

Verdon G, Albers SV, Dijkstra BW, Driessen AJ, Thunnissen AM (2003) Crystal structures of the ATPase subunit of the glucose ABC transporter from *Sulfolobus solfataricus*: nucleotide-free and nucleotide-bound conformations. *J Mol Biol* **30:** 343–358

Vergani P, Lockless SW, Nairn AC, Gadsby DC (2005) CFTR channel opening by ATP-driven tight dimerization of its nucleotide-binding domains. *Nature* **433:** 876–880

Vergani P, Nairn AC, Gadsby DC (2003) On the mechanism of MgATP-dependent gating of CFTR Cl− channels. *J Gen Physiol* **121:** 17–36

Wang W, Oliva C, Li G, Holmgren A, Lillig CH, Kirk KL (2005) Reversible silencing of CFTR chloride channels by glutathionylation. *J Gen Physiol* **125:** 127–141

Wu J, Kaback HR (1997) Helix proximity and ligand-induced conformational changes in the lactose permease of *Escherichia coli* determined by site-directed chemical crosslinking. *J Mol Biol* **270:** 285–293

Yuan YR, Blecker S, Martsinkevich O, Millen L, Thomas PJ, Hunt JF (2001) The crystal structure of the MJ0796 ATP-binding cassette. Implications for the structural consequences of ATP hydrolysis in the active site of an ABC transporter. *J Biol Chem* **276:** 32313–32321

Zaitseva J, Jenewein S, Jumpertz T, Holland IB, Schmitt L (2005) H662 is the linchpin of ATP hydrolysis in the nucleotide-binding domain of the ABC transporter HlyB. *EMBO J* **24:** 1901–1910